Chapter 2

Background and Review

2.1 Targeted Cancer Nanotherapies

Therapies such as chemotherapy or small molecule molecularly targeted therapeutics (e.g.kinase inhibitors) are powerful anticancer treatments and form the standard of care in current clinical management of cancer. However, these agents distribute non-specifically in the body, and since cancer targets are often the overexpression of normally expressed markers, these agents can cause toxicity to both cancer and normal cells. Treatment-associated toxicity (TRT) can limit achievable dosage within the tumor and result in suboptimal treatment. Furthermore, many tumor types can develop resistance to these small molecule therapies.

Nanotherapies, which describes the class of agents with a size range of ~1–100 nm, are being actively explored to overcome the issues of small molecule therapies [21, 4, 22]. Often, small molecule therapies are directly attached or encapsulated within a "carrier" nanostructure for drug delivery. Structures being explored range from polymers [23, 24] and carbon nanotubes [25] to liposomes [26] and viral protein cages [27]. Gold nanorods can be delivered to the tumor to provide localized photothermal heating. This can cause direct tumor toxcity or improved uptake of a complementary drug carrier [7]. Alternatively, existing peptides and protein constructs can be modified to improve their targeting efficacy. An example of this is the development of immunocytokines, whereby cytokine peptides are engineered onto antibodies to target their effects locally to the tumor site [28, 29].

Nanotherapies overcome toxcity and resistance issues by several mechanisms. First, size and surface characteristics of nanotherapies can be tuned to extend their circulation time in the body

by reducing reticuloendothelial and renal clearance. Next, the nanotherapies can target the tumor by harnessing the properties of the tumor environment. The most characterized property is the enhanced permeability and retention effect (EPR). The fast growing tumor requires a continuous nutrient supply and thus releases factors to recruit and grow blood vessels. Imbalance of angiogenic signals lead to highly disorganized and leaky tumor blood vessels. This, along with compromised tumor lymphatics, allow macromolecules above ~50 kDa to accumulate in the tumor interstitium. The nanotherapy considered in this work, CRLX101 [30], has been postulated to accumulate via EPR (see chapter 4 for further discussion).
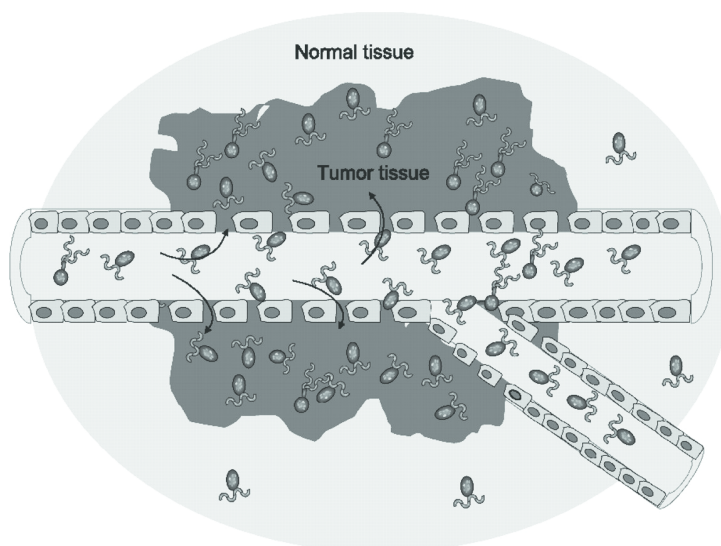

Figure 2.1: Enhanced permeability and rentention. Dysregulation of the angiogenic signals within tumors lead to immature and leaky blood vessels in the tumor. This enables macromolecules and nanoparticles to enter the tumor interstitium. This, along with compromised lymphatics, lead to retention of these large-sized particles in the tumor (adapted from [4]).

Tumor targeting can be further improved. Specific targeting of cell populations via receptor targeting can be achieved by the attachment of receptor ligands or antibody fragments onto the nanotherapy surface. Transferrin or folate receptors, which are often over-expressed in tumors, are common targets [31, 32]. Targets along the tumor endothelium (e.g. $\alpha_v\beta_3$ integrin receptors) have also been explored for antivascular agents [33]. Other properties, such as the pH of the tumor [34] and the overexpression of enzymes [35] in the tumor have also been explored as tumor localizing targets. Recent work suggests that combining several of these targeting mechanisms into a single nanotherapy system is synergistic [7].

Tumors can become chemoresistant via multiple mechanisms. The best known is the P-glycoprotein efflux pump pathway [36]. Nanotherapies can potentially overcome these effects since they uptake into cancer cells via different pathways compared to conventional therapies [37].

2.2 Modulation of the Tumor Microenvironment to Enhance Drug Uptake

Improved tumor targeting is the primary rationale behind the development of cancer nanotherapies [38]. However, nanotherapies currently in clinical trials show modest improvements over conventional treatment [39]. Studies exploring the factors preventing enhanced efficacy have highlighted the heterogeniety of nanotherapy uptake within the complex tumor microenvironment. Although leaky blood vessels form the basis of EPR, their vessel-wall structure are often abnormal, leading to vessel collapse and thus hetereogeneous delivery [40]. Similarly, lymphatic drainage is also compromised in tumors with a result of fluid retention within the tumor mass and tumor intersitial hypertension [41]. This may impede penetration of nanotherapies throughut the tumor. Moreover, the tumor microenvironment consists not only of tumor cells, but support matrix such as collagen fibers and glycosaminoglycan [15, 42]. Depending on the size and structure of nanotherapies these structures (which are also heterogeneous within the tumor) can impede nanotherapy penetration and limit their efficacy [18].

Strategies have been investigated to modulate the tumor in order to improve nanotherapy penetration. Judicious use of antiangiogenic agents have been used to "normalize" tumor blood vessels [43]. This improves vascular perfusion within the tumor and reduces interstitial fluid pressure. However, these effects may be transient and actually remove the leakiness desired from EPR. The leakiness of the blood vessel have also been modulated via other means, such as the application of VEGF or metronomic chemotherapy regimens [44, 45]. The tumor matrix can also be modulated via degradation of the collagen matrix and decreasing the levels of glycosaminoglycans, improving the uptake of antibodies and viral particles [46, 42].

Another strategy to improve therapy uptake in the tumor is the use of cell-penetrating peptides. Peptides are generated with specific targets such as tumor blood vessels or the cell nucleus, most

often via phage display [47]. These peptides are then often fused to a cargo of interest, such as nanoparticles or siRNA to improve the drug or particle uptake [48]. Interestingly, a recent paper reports that a tumor-penetrating peptide (iRGD) can improve the uptake of a variety of drug therapies ranging from small molecules to nanoparticles into tumors without direct conjugation to the agent of interest [49]. This suggests that iRGD has tumor modulating effects beyond pure tumor homing. Although the exact mechanism of action *in vivo* remains elusive, iRGD is purported to target the tumor via the α_v integrin receptors on tumor blood vessels. A cleavage mechanism then occurs, exposing a peptide modif (the CendR motif [50]) which interacts with the neuropilin-1 receptor and mediates downstream effects leading to drug tumor penetration [48, 49, 50]. Neuropilin-1 is associated with the VEGF pathway suggesting that modulation of tumor blood vessels may play a role in this process. The imaging of iRGD effects were investigated in this work. Further discussion of iRGD is found in chapter 5.

2.3   Imaging in Oncology

The research and clinical management of cancer has been revolutionalized by imaging [12]. Currently, several imaging modalities are being developed and used. For successful translation of imaging assays from the benchtop to bedside, it is imperative that all aspects of the imaging assay be considered, ranging from the biological process being considered, the chemistry of the probes and the imaging hardware, to the methods of image analysis [51].

Here, we review imaging considerations with regards to the two modalities considered in this work: PET and MRI.

2.3.1   PET Basics

PET is an imaging technique that relies on the emission of coincident annihilation photons emitted indirectly from positron emitting radionuclides [52]. Attachment of radionuclides to specific biological molecules or compounds can provide highly sensitive assays of many physiological processes [51]. The biodistribution of these molecules in the body are dependent on their pharmacokinetics and pharmacodynamics. PET images showing their biodistribution allow us to infer the mechanism of specific physiological processes in a dynamic and noninvasive manner. Radiolabelled compounds

have been developed to monitor many processes including metabolism [53, 54], receptor binding [55, 56], antibody trafficking [57], gene expression [58], and perfusion [59].

As the unstable radionuclide attached to the molecule of interest decays, positrons are emitted as byproducts. The positron travels a short distance (*the positron range*), losing its kinetic energy, and then annihilates with an electron. The annihilation process converts the masses of the positron and electron into two 511 keV photons emited in coincidence almost simultaneously (~nanoseconds, ns). Detection of these photons defines a line volume (*line of response*) along which the annihilation process occurred. Detection of these photons at multiple angles around the object allows the definition of multiple line integrals of activity distributions. Image reconstruction algorithms [60, 61] can be applied to this information to create images of radioactivity distribution (and hence the molecules attached). The spatial resolution of PET systems is on the order of ~1–5 millimeters and is a function of the positron range, deviations from colinearity of emitted coinicidence photons, and the effectiveness of the detector to resolve lines of response.

With proper correction and calibration of the line integral data and reconstructed image data, the pixel intensities of resultant images should be proportional to the radioactivity present at the pixel location and thus would provide implicitly the concentration of the radiolabelled probe of interest. For further discussion of both hardware and software calibration required for well-calibrated PET, we refer the reader to [52, 51] and chapter 3.

As discussed earlier, successful PET studies require prudent integration of hardware, software, biology and chemistry. Of interest to the work described herein is the need to choose the correct radioisotope to explore the physiological processes of interest. Several positron-emitting isotopes are currently routinely used in PET (table 2.1). Three important factors need to be considered in choosing the isotope for any study:

1. *Chemistry*: Different radioisotopes are linked to the molecule of interest with a variety of methods. Halogens such as ^{18}F and ^{76}Br are covalently linked to the molecule, while radio-metals such as ^{64}Cu and ^{68}Ga [62] are conjugated to the molecule via a chelate (such as DOTA) [63]. Careful consideration needs to be made to determine whether the molecule of interest can be labeled with the isotope, and whether chemistry of the labelling will affect the pharmacokinetics or biological interpretation of the PET signal. Moreover, while the

chemistry of radioisotopes are the same as the non-radioactive isotopes, the radiolabelling process needs to be well within the half-life of the isotope of interest to allow enough signal for imaging.

2. *Half–life*: The half-life of the isotope needs to be fitted to the physiological question of interest. For example, the kinetics of nanotherapies are on the order of hours to days. If the question at hand is to determine the kinetics of the agent, then a relatively long half-life isotope such as ^{64}Cu or ^{124}I would be desirable. However, a short half-life isotope such as ^{18}F or ^{11}C may be more applicable for fast acting physiological processes or diagnositic purposes, where radiation overexposure becomes a critical concern.

3. *Branching fraction*: The branching fraction for a isotope defines the fraction of particles which will decay via a particular decay mode. Specifically, we are concerned with the percentage of positron emission. One may need to design imaging protocols, the injected dose or make alterations to the calibration to account for the lower sensitivity of certain isotopes during PET imaging. This is particularly relevant for ^{64}Cu, as only 17% of all decays are positrons.

Table 2.1: Common positron-emitting isotopes

Isotope	Half-life (hours)	β^+ decay fraction (%)	β^+ energies (keV)
^{68}Ga	1.13	90	1899
^{11}C	0.34	99	960
^{15}O	0.034	99	1732
^{18}F	1.83	100	634
^{64}Cu	12.7	17.4	653
^{61}Cu	3.3	62	1220
^{76}Br	16.2	6.3	871
		5.2	990
		25.8	3382
		6	3941
^{89}Zr	78.4	22.7	897
^{86}Y	14.7	11.9	1221
		5.6	1545
^{124}I	100.3	11.8	1535
		10.9	2138

2.3.2 MRI Basics

MRI leverages the quantum mechanical phenomenon whereby nuclei with non-zero magnetic spin quantum numbers achieve splitting of spin energy levels when placed in an external magnetic field. Classically, one can visualize this spin property as a charge rotating about an axis. This rotation creates a small magnetic moment (dipole) that can be characterized by a vector. In the absence of an external magnetic field, the dipoles are randomly orientated and the vector sum of the dipoles within a region (e.g.an imaging voxel) is zero. When placed in an external magnetic field, the dipoles align to the field parallel or antiparallel to the field, corresponding to different energy levels. An excess of spins align in the lower energy state, resulting in a net magnetization vector aligned with the external B_0 field. The aligned spins precess about the field axis with a fixed angular frequency ω and is related to B_0 by the Lamor equation:

$$\omega = \gamma B_0, \tag{2.1}$$

where γ is the gyromagnetic ratio for the nuclei in question.

When aligned, the magnetization "signal" from any population of spins cannot be differentiated with the stronger B_0 field. To detect the magnetization signal, spins need to be "tipped" from the longitudinal to the transverse plane. This can be achieved by excitation of the spins with RF pulses at the Larmor frequency ω. Energy released as excited spins relax back to the longitudinal plane can be detected using receiver coils to general a MR signal.

Differentiation of different types of nuclei and substances are determined by their frequency of precession about B_0, and their characteristic relaxation signature after excitation. Traditionally, the two major relaxation rates examined are T_1, the rate at which the longitudinal magnetization recovers post RF excitation and T_2, the rate at which the magnetization in the transverse plane disappears [64]. A number of other relaxation mechanisms have also been described [65]. Different tissues (e.g.fat, water) have their own characteristic T_1 and T_2 values, which can alter depending on changes in temperature and structure.

Finally, this information can be combined with spatial encoding techniques to generate a MR image. Magnetic gradient fields can be introduced across a tissue sample, encoding each location with specific frequency and phase information. Knowledge of this enables decoding of the RF

relaxation information across the tissue sample in three dimensions.

Conventional MRI combine RF pulsing and gradient encoding together into a MRI *pulse sequence* to generate images. Combined with knowledge of the relaxation behavior of different tissues and structures, one can design and alter multiple parameters in pulse sequences to achieve certain image contrasts. The reader is referred to the following texts for a more detailed treatment [66, 64, 67]. Here, we discuss in particular two functional MRI techniques used in the work herein.

2.3.2.1   Diffusion MRI

Diffusion is the random movement of particles from regions of higher concentration to regions of lower concentration. Biologically, we are mostly concerned with the movement of water. Diffusion of water *in vivo* is not free; fiber tracts in the brain, intact cell membranes and structural tissues can restrict water diffusion in single or multiple directions.

MRI methods have been developed to produce *in vivo* images that are sensitive to the diffusion of (mainly) water. As discussed above, traditional anatomical MRI image contrast is determined by the relaxation characteristics of the tissue being imaged. Consistency of proton spin precession relies on the presence of a homogeneous magnetic field. If during the pulse sequence an extra gradient pulse is applied, the field is distorted and proton spins begin to disperse in phase. This dispersion can be reversed by the application of another gradient pulse opposite in magnitude to the first pulse to rephase the spins. However, this rephasing will be imperfect for spins that have diffused along the direction of the gradient pulse during the time interval and will lead to signal loss. The diffusion sequence was developed for NMR by Stejskal and Tanner [68] and adapted for MRI by Le Bihan (figure 2.2) [69]. The equation governing the signal from this sequence is:

$$S = S_0 e^{-bADC},\tag{2.2}$$

where S_0 is the signal intensity with no diffusion weighting, S is the signal with the diffusion gradient applied, b is a scaling factor that incorporates the effect of gradients in the sequence and ADC, the apparent diffusion coefficient, is the aggregate diffusion coefficient value calculated from the imaging voxel. The ADC can be calculated by acquiring images at multiple b values and performing a curve fit.

In recent years, more complicated models of diffusion have also been applied to this to analysis the diffusion data, probing different compartments and aspects of the *in vivo* diffusion process [70, 71, 72, 73, 74].
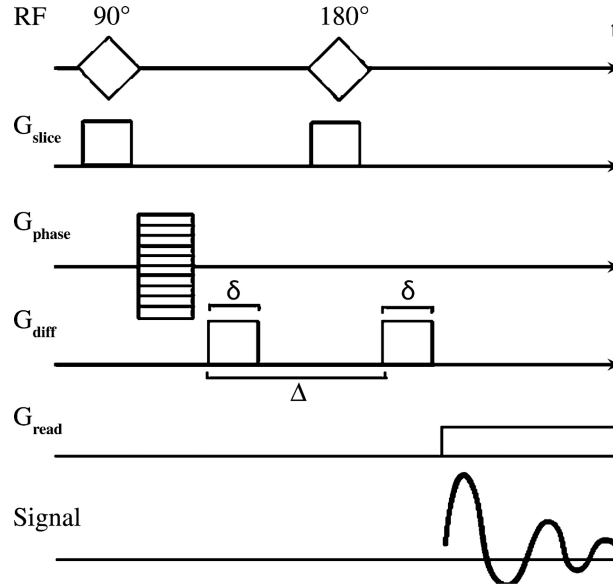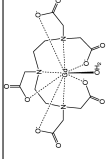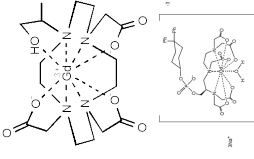

Figure 2.2: A basic pulsed gradient SE sequence for diffusion MRI imaging. Two diffuson gradients (G_{diff}) are incorporated into a standard SE sequence sensitive to different diffusion rates along the gradient direction. δ = duration of the diffusion-encoding gradient, Δ = diffusion time interval, G_{phase} = phase-encoding gradient, G_{read} = readout gradient, G_{slice} = section-selective gradient. These aquisition parameters are encapsulated into the *b* factor described in the text (adapted from [73]).

2.3.2.2 Dynamic-Contrast Enhanced MRI (DCE-MRI)

Conventional MRI provides high resolution images of anatomy. Paramagnetic contrast agents can alter local tissue relaxation parameters to aid image contrast enhancement and highlight specific structures. Many different MRI contrast agents have been developed (table 2.2) which can alter tissue T_1 or T_2. DCE-MRI most commonly refers to MRI that dynamically alter the T_1-weighting of tissues [75, 76, 77].

These contrast agents have characteristic pharmacokinetic properties, which researchers and clinicians have harnessed to study the functional properties of tissues. Most commonly, contrast agents are injected intravenously and a time series of MRI images are acquired to follow the wash-in and wash-out of the contrast agent. The vascular function of tissues such as viable tumors and

Table 2.2: Some MRI contrast agents considered in this work

Name	Formula	Structure	Molecular weight	$r_1(B_0)$ (mM/s)	$r_2(B_0)$ (mM/s)
Magnevist	$C_{28}H_{54}GdN_5O_{20}$		938 g/mol	3.4 (1T)	3.8 (1T)
Prohance	$C_{17}H_{29}GdN_4O_7$		558.68 g/mol	3.7 (1T)	4.8 (1T)
Ablavar	$C_{33}H_{40}GdN_3Na_3O_{15}P$		975.88 g/mol	19–28 (1.5T)	
Ferumoxytol	$Fe_{5874}O_{8752} - C_{11719}H_{18682}O_{9933}Na_{4414}$		750 kDa	40 (0.47T)	160 (0.47T)
Albumin-(Gd-DTPA)35			107 kDa	14.8 (0.25T)	388 (0.25T)

livers can be inferred by the behavior of the contrast agent over time (figure 2.3). Other studies have also used contrast agents to study the dynamics of cellular processes like inflammation [78] and pharmacological response [79].

Several methods can be applied to analyze DCE-MRI [80, 81, 82]. Most were adopted from the field of nuclear medicine. Semiquantitative metrics such as the area under the curve (AUC), the slopes of contrast agent (CA) uptake and washout curves as well as the peak CA uptake have been applied to DCE-MRI. Alternatively, quantitative metrics based on pharmacokinetic modeling can be derived. The most widely used model is the two-compartment Kety model from which volume transfer constants (K_{trans}, k_{ep}) between compartments and volume of the tissue compartments (v_e, v_p) can be calculated.

It is important to remember that the image enhancement observed in these studies are not a direct measure of [CA], but the enhancement due to water exchange with CA. Recently, the effects of water-compartmentalization on CA-water exchange have been studied. Kinetic models which consider these trans-cytolemmal effects have been proposed and explored for DCE-MRI analysis [83, 84, 85, 86].
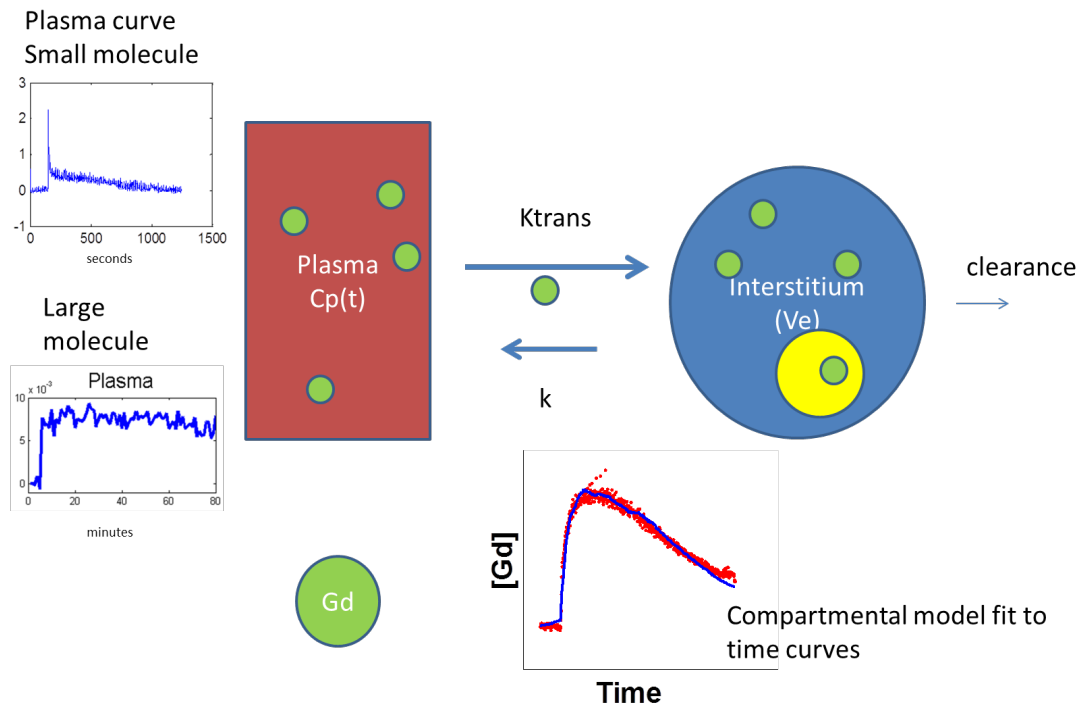
Figure 2.3: DCE-MRI can infer tissue vascular function. MRI-visible contrast agents injected intravenously can be visualized by MRI in plasma and also vascularized tissues. The pharmacokinetics of the image enhancement is related to the structure of the CA (e.g.small molecule CA have fast first-pass circulation vs. large molecule CA). Image enhancement curves can be fitted to pharmakinetic models to infer quantitative parameters of vascular function. Shown here is the commonly used two-compartment model.

2.3.3   Combining PET and MRI

2.3.3.1   Why Hybrid PET/MRI?

While both PET and MRI are powerful imaging modalities individually, each has their own strength and weaknesses. These are summarized in table 2.3.

Table 2.3: Comparison between PET and MRI

	PET	MRI
Strength	Very sensitive (~nM)	high-resolution soft–tissue and anatomical information (<1 mm)
	Can monitor multiple biological processes	Metabolic (MRS) and physiological information available (e.g.diffusion, DCE-MRI)
		Multiple contrast mechanisms: flexible
		No ionizing radiation
Weakness	Poor spatial resolution (~1–2 mm)	Not sensitive (~mM)
	Limited anatomic information	Multiple contrast mechanisms: complicated
	Ionizing radiation	

From the table, it is clear that PET and MRI are quite complimentary and information from the two modalities should be synergistic [14]. Yet, this alone would not justify the efforts to develop integrated systems. The key advantage of integrated systems is the ability to obtain simultaneous (or near-simultaneous) PET and MRI information. Here, we discuss why the integrated approach is worthwhile.

There are several reasons why integrated PET/MRI is useful. Although mundane, the ability to acquire two images at once can save time, which is important both in the lab and the clinic. Further, one modality can aid the image quality of the other. The most obvious application has

been the use of MRI information to improve PET quantification. MRI data can offer information for attenuation correction [87, 88] and motion correction [89]. Hybrid PET/MRI systems can also be combined with bimodal PET/MRI probes to quantify tissue CA uptake and aid interpretation of the CA imaging signal [90]. In all of these cases, robust coregistration of the PET and MRI image space enables MRI data to directly correct the PET data.

Ultimately though, it is the physiological applications possible with PET/MRI that will drive the widespread adoption of PET/MRI technology. subvoxel coregistration in space, which is difficult to achieve especially outside the head, enables us to make solid biological inferences between spatial distributions observed in PET and MRI at a fine scale. This aspect of PET/MRI integration forms the scope of our investigations in chapter 3. Synchrony of the PET and MRI signals enables us to make inferences between PET and MRI assays of time-sensitive physiological processes: this is the motivation for the investigations in chapters 4 and 5. The ability to obtain the two modalities in near real-time also enables the information obtained from one modality to drive studies performed with the alternate modality and vice versa (figure 2.4).
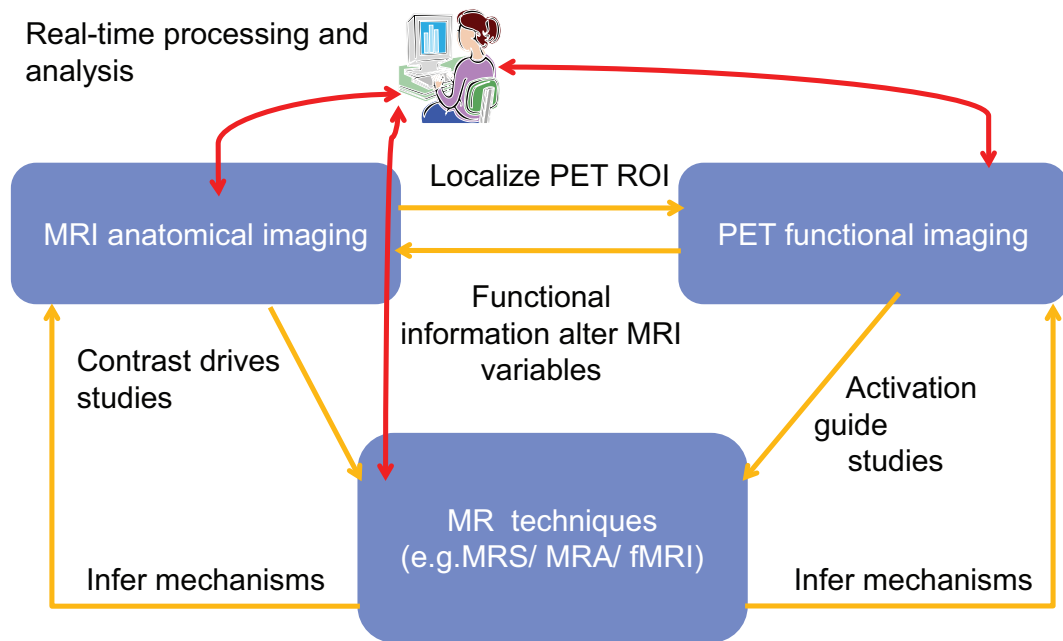

Figure 2.4: Real-time paradigm for PET/MRI studies.

2.3.3.2 Current State of Hybrid PET/MRI Systems

Current approaches for hybrid PET/MRI systems are summarized in table 2.4. Four main approaches are followed:

1. Sequential PET/MRI with PET and MRI hardware separate from each other.

2. Sequential PET/MRI with integrated PET/MRI hardware, but powered separately.

3. Simultaneous PET/MRI with radical redesign of MRI and PET hardware.

4. Simultaneous PET/MRI with novel PET hardware to fit in conventional MRI (PET insert).

The PET/MRI system developed in this work is the PSAPD-based PET insert (figure 2.5) [105]. Detailed description about the system implementation is described in [106] and chapter 3.
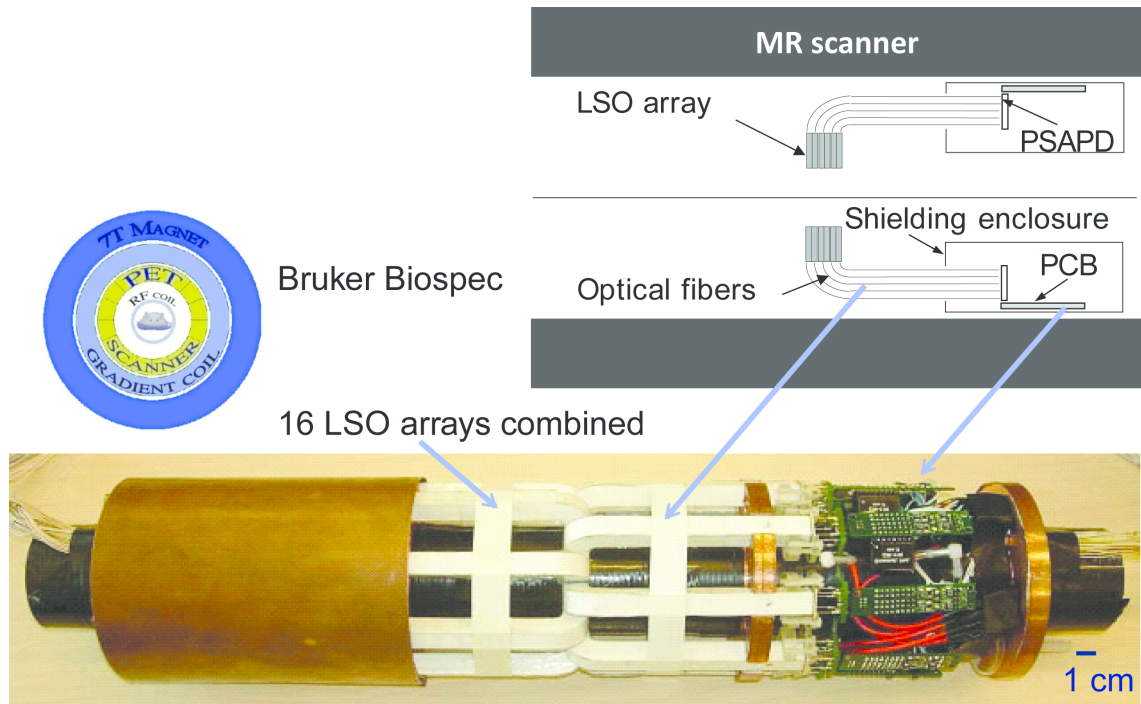

Figure 2.5: PSAPD-based MR-compatible PET insert. The insert consists of 16 LSO-PSAPD detectors arranged in a single ring. The insert is placed inside the bore of a 7 T small animal MRI. The RF coil and animal subject is placed in the PET insert.

2.3.4 Digital Whole-body Autoradiography

Digital whole-body autoradiography (DWBA) is used as an *ex vivo* assay of radioactivity distribution in tissues [107, 108, 109]. The tissue of interest is sliced and placed onto the DWBA phosphor

Table 2.4: Current state of hybrid PET/MRI systems

Approaches	Description
Sequential PET/MRI, separate hardware	Sequential clinical PET/MRI system. Mature PET and MRI technologies integrated with a moving patient table (Phillips, Netherlands) [91, 92].
Sequential PET/MRI, separate powering	Field-cycling method whereby the MRI field is turned on for MRI acquisition then turned off for PET acquisition. MRI and PET are integrated, enables conventional PET PMT detectors to be used. MRI works at low field (0.3 T) [93].
Simultaneous PET/MRI with radical redesign of MRI and PET hardware	Design of a split-magnet to house extended PMT PET detectors. MRI and PET are integrated, mature PET PMT detectors designed into the system. MRI works at low field (1 T) [94].
	Integrated clinical whole-body PET/MRI system consisting of APD-based detectors housed between RF coils and MRI gradients (Siemens, Germany). MRI and PET are integrated [95] .
Simultaneous PET/MRI with novel PET hardware to fit in conventional MRI	PMT-based ring inserts placed inside a open 0.2 T , 0.3 T and 3 T MRIs. Long fiber-optic cables are used to couple the scintillation elements to the PMTs and electronics [96, 97, 98, 99].
	APD-based head insert for 3 T clinical MRI (Siemens, Germany). The FOV is limited to the brain [100].
	APD-based PET ring system based on the RatCAP PET, can be placed in 9.4 T MRI. Insert can be removed [101].
	Integrated PET insert based on APD-LSO detectors, developed for small animal 7 T MRI. Insert can be removed [102].
	SiPM-based PET ring insert for small animals, tested in clinical 3 T and 0.15 T MRI. Inserts can be removed [103, 104].
	Integrated PET insert based on PSAPD-LSO detectors, developed for small animal 7T MRI. Insert can be removed [105].

imaging plate. The phosphor imaging plate is designed to detect high energy radiation. Excitation of the BaFBr:Eu^{2+} crystals on the plate causes oxidation from Eu^{2+} to Eu^{3+} and the trapping of the electron in the "color-center" of the $BaFBr^-$ complex. The plate can be read by shining red light (~633 nm) onto the plate and imaging the photon released during Eu^{3+} reduction back to Eu^{2+} [110].

DWBA has been used extensively in pharmaceutical research to study drug distributions and receptor binding. It has been used to verify isotope distributions observed in PET [111]. This is aided by DWBA's relatively high spatial resolution (~100 mm) and high sensitivity. The same tissue of interest can be imaged by DWBA several half-lives after a PET study to verify biodistribution [112], and forms an ideal "gold-standard" for PET.

2.3.5 Imaging of Targeted Nanotherapy Uptake

Knowledge of the biodistribution of targeted therapies is traditionally performed from *ex vivo* assays. Drug kinetics are determined by measuring drug content in tissues of interest (in animals) harvested at specific time points [113, 30]. However, a wide intersubject variability of drug uptake may exist and thus requires a large number of animals to make robust statistical inferences. Increasingly, these data are being complemented by *in vivo* imaging data [114, 19] that can be acquired longitudinally within single subjects. Biodistribution studies of radiolabelled antibodies and nanoparticles can be peformed using PET or SPECT due to the high sensitvity of radioactivity [115, 116, 117, 118]. Although MRI is a less sensitive modalitity, researchers have also developed MRI approaches to monitor the targeting of nanotherapies in the tumor [119]. MR-visible agents can be linked to tumor-targeting antibodies [120] and nanoparticles [121, 48] and can utilize intrinsic properties of tumors (e.g.the presence of certain enzymes like matrix metalloproteinases) to activate the localized signal [35].

Most of these studies focus on imaging the gross uptake of targeted therapies into tumors, that is, whether the therapy will reach and stay in the tumor. However, there is recent interest in understanding how the tumor microenvironment may modulate this uptake intratumorally. *Ex vivo* studies suggest that uptake of targeted nanotherapies can be related to structrual factors such as the distribution of blood vessels [113, 122]. Kobayashi *et al.* observed that MRI of breast tumor mouse models showing different vascular structures can be correlated with gross tumor antibody

uptake [123]. Thurber and colleagues have begun to investigate these factors by developing models to explain these distributions and verifying these models with fluorescent imaging [16, 20, 124]. Imaging studies that enable the dynamic visualization of the tumor microenvironment (which can be probed by MRI and PET) in concert with the distribution of the targeted therapy will contribute to the development of these models for clinical application.

2.3.6   Imaging of Targeted Nanotherapy Response

At present, clinical imaging of tumor response to targeted nanotherapies focuses on evaluating size changes of tumors as determined by the RECIST criteria [11]. Tumor size and growth are evaluated using MRI or PET/CT to monitor changes in size [125, 126]. This mirrors the standard of care for evaluating small molecule chemotherapy response. For example, the clinically approved liposomal formulation of doxirubicin (Doxil) has been monitored by PET/CT in phase I/II studies [127, 128], while albumin-bound palitaxel (Abraxane) have been followed by PET/CT and MRI [129].

Functional imaging techniques, such as diffusion MRI [130], DCE-MRI [131] and ^{18}F-FDG-PET and ^{18}F-FLT-PET [53] and are being investigated for early treatment monitoring for small molecule anticancer drugs. These techniques have the ability to determine changes in the tumor prior to tumor size changes, and to probe changes of biological processes within the tumor. Moreover, such functional imaging data can be applied to models of tumor growth to enable prediction of tumor response [132, 133]. DCE-MRI have been used to evaluate responses to bevacizumab and its antivascular effects [134]; but fewer preclinical [126, 135, 136] or clinical studies have been pursued to investigate the utility of such techniques to monitor tumor response in other nanotherapies. The reader is referred to chapter 4 for further discussion of this topic.